Design of an Integrated Inductor for 45kW Aerospace Starter-Generator

M. Raza Khowja*, C. Gerada*+, G. Vakil*, S. Quadir Quadri*, P. Wheeler* and C. Patel*
Power Electronics, Machines and Control (PEMC) Group
The University of Nottingham, UK* & CHINA+

***Abstract* – A close physical and functional integration of passive components is required to make an efficient and power dense overall system. Such power dense systems are a prerequisite in aerospace and marine applications. This paper presents a design of an integrated rotor-less inductor for the application of a 45kW aerospace starter-generator. The impact of high current density inductor is investigated and compared with traditional *EE* core inductor in terms of total weight and volume. Both inductors are sized using area product approach and its design parameters are validated using finite element analysis. Comparative analysis between the traditional *EE* core and the integrated inductor has shown a significant reduction in total weight and volume. The total weight of the integrated inductor is reduced by 55.4% whereas the total volume is reduced by 52.7% when compared to traditional air cooled *EE* core inductor.**

***Index Terms* — EE Core Inductor, Integrated Inductors, Integration of Passives, Rotor-less Inductor, Aerospace Applications and Starter-Generator.**

I. INTRODUCTION

Passive filter components such as filter inductors and capacitors occupy a substantial amount of space in electric motor drives which add the penalties of increased system losses and its associated weight. In a conventional approach, the filters are designed and introduced separately after the drive system components have been defined. This leads to discrete sub-systems which require a functional and structural integration of each sub-system in order to make an efficient and power dense overall system. Such power dense system is vital in aerospace and marine applications [1-5]. In order to overcome these drawbacks, the integration of passive components need to be introduced both from functional and physical point of view [1-5].

There are many possibilities in aircraft drives system to integrate the passive components. The integration of passive components in such systems offer many benefits such as power dense design, reduction in cost, mass, size and eases manufacturing process. Thus, applications where high power density is needed, integrative approach seems to be the best solution.

This paper will look into a design of an integrated rotor-less inductor which was proposed in [2-5] for a 45kW aerospace starter-generator. This paper investigates the impact of high current density on the inductor design, effectiveness of integration and compares its design with traditional *EE* core air-cooled inductor in terms of its weight and volume. Both integrated and traditional inductors are modelled and analysed through finite element analysis (FEA).

II. LITERATURE REVIEW

A. Traditional Filter Inductors

Fig. 1 shows the traditional shapes and designs of the filter inductor. In common practice, different type of cores has been used for fabricating inductors which includes: tape wound, powder and laminated cores [6].

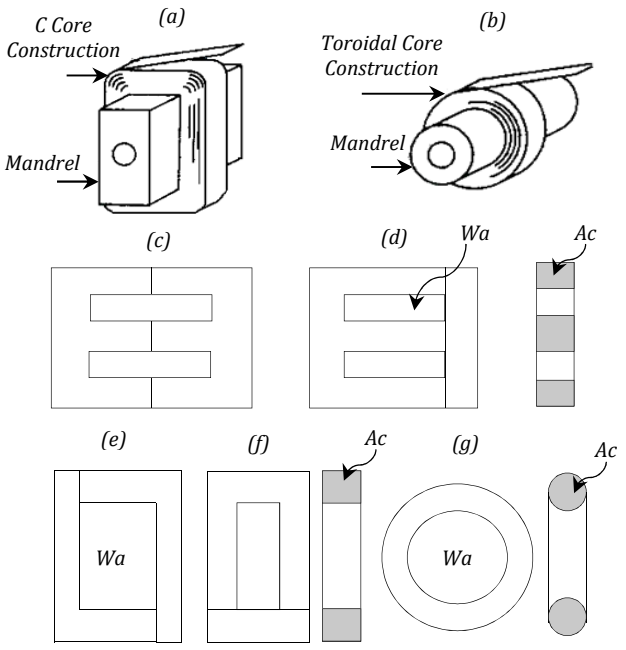

Fig. 1. Construction of Conventional Inductors (a) C core (b) Toroidal Core (c) EE core (d) EI core (e) LL core (f) UI core (g) Toroidal Core

Air core does not use the steel material. The coils are wound on non-magnetic formers such as plastic or ceramic. The drawback of air-cored inductor is that they are less permeable than steel material. However, they are often adopted in high frequency applications where core losses need to be avoided which are dependent on frequency squared [6-8].

Tape wound cores are manufactured by winding the copper tape/wire around a mandrel. A magnetic material in the form of preslit tape as shown in Fig. 1(a) and (b). The benefit of using this type of core is that flux is parallel with the direction of

rolling of the magnetic material, which allows to setup maximum flux with minimum field strength. Tape wound core can be constructed with C, EE or toroid cores [6].

Powder cores are very unique as they have inherent airgap which is evenly distributed throughout the core material. This acts in a similar way as a core with airgap which reduces the core saturation at higher levels of current. They come in a variety of materials and are very stable with temperature. They can be toroid, EI or EE in construction [6].

The laminated cores are one of the most commonly used cores in power electronics and motor drive applications. Laminated core consists of pressed steel sheets with the coating of insulation on the surface. The insulation coating reduces the eddy currents between the sheets. The laminated cores can also be EE, EI, LL, UI and toroid in construction as shown in Fig. 1(c)-(g) [6].

B. Integrated Filter Inductors

Recently, the passive integration has been a prime focus in power electronics and motor drive application that has resulted in an overall compact and power dense system. In [2], a novel approach to integrate the inverter output filter inductor is presented for PMSM motor drives. The proposed motor uses the inherent motor magnetics as a filter inductance instead of using an external filter inductor. This leads to the elimination of power losses and its associated weight and volume.

The author of [3-5] introduced the novel options to integrate the passive filter inductors within the housing of the electrical machine as shown in Fig. 2. The novel options include: motor-shaped rotational inductor and motor-shaped rotor-less inductor. Both inductors are integrated axially on the same shaft, inside the motor housing which results in a shared cooling system and hence, eliminates the requirement of a separate cooling system. The rotor of the rotational inductor rotates at the synchronous speed of the stator magnetic field to minimize the magnetic losses in the rotor.

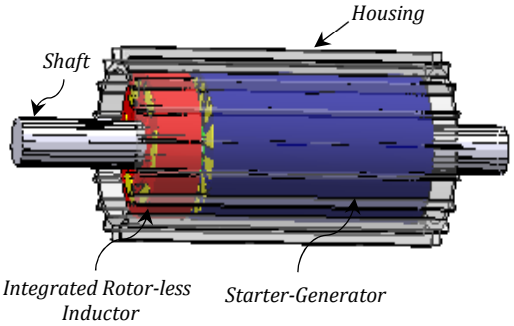

Fig. 2. Radial Cross-section and Flux Distribution (a) EE Core Inductor

On the other hand, rotor-less inductor is having the similar structure without rotor which makes it suitable for DC-Link smoothing inductors, grid input filters and isolation transformers. In contrast, the rotational inductor can only be adopted for the applications of high speed inverter motor drives.

In [9-12], the perspectives on the integrated filter inductors are presented, that motivates the drive integration on a system level. The design of integrated filter inductor for power factor correction application is presented in [9]. The paper modified the stator laminations to increase the stator back iron which acts as an integrated filter inductor. This modification increases the outer diameter of the motor.

In [10-11], the entire stator back iron is utilized as a magnetic part for one or more discrete inductors by integrating toroidal winding which pushes the alternating magnetic flux in the complete loops through the back iron of the stator core. If the stator back iron of the machine is operating linearly then the presence of ring flux due to toroidal winding will not affect the main flux. But in physical prototype because of nonlinearity the back iron thickness has to be increased.

The principle of electromagnetic integration is used for integrating capacitor in the same magnetic component as that of the inductor. The integrated filter is the planar integrated L-C winding, which consists of a dielectric substrate with conductor windings directly deposited on both sides, thus resulting in a distributed inductance and capacitance structure. Moreover, different equivalent circuits can be achieved by connecting the terminals of integrated LC structure in an appropriate manner [12-18].

The same principle of [12-18] is applied for C-core EMI inductor in [19-20]. The distributed capacitance is implemented in the conventional way, whereas the inductor is implemented by utilizing the cathode and anode foils of the capacitor to form the windings. The windings are then enclosed in a can, which has a hole in the middle for the magnetic core.

III. AREA PRODUCT APPROACH

The voltage induced on the inductor terminals can be obtained by referring to Fig. 3 while assuming the terminal voltage and current through the inductor is sinusoidal. The expression for induced voltage is,

$$V_{peak} = N_{ph}\varphi_{peak}\omega_s \tag{1}$$

$$V_{rms} = K_w N_{ph} B_{peak} A_c f_s \tag{2}$$

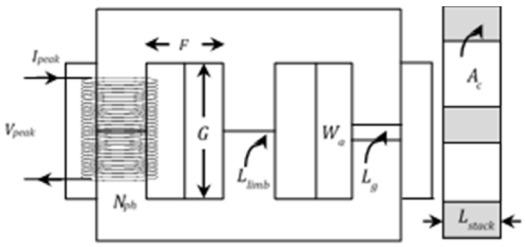

Fig. 3. Physcial Layout of 3 Phase EE core Inductor

Where K_w, A_c, φ_{peak}, B_{peak}, f and N_{ph} are waveform factor, cross-sectional core area, magnetic flux, peak flux density of the magnetic core, source frequency and number of turns per phase respectively.

The phase turns of the inductor for a given window and conductor strand area can be determined by,

$$N_{ph} = \frac{K_f W_a}{A_w} \tag{3}$$

Where, K_f is the window fill factor which is defined by the ratio of copper area to the window area. W_a is the window area and A_w is the conductor area.

In practice, for inductor, window fill factor typically varies from 0.4 to 0.6 to provide enough space for wire insulation, bobbins, slot liner and air space between the insulated wire turn. By substituting the Eq. 3 in Eq. 2, we have,

$$V_{rms} = \frac{K_f K_w B_{peak} A_c W_a f_s}{A_w} \tag{4}$$

By multiplying the RMS current through the inductor on both sides, we have,

$$V_{rms} I_{rms} = \frac{K_f K_w B_{peak} A_c W_a f_s I_{rms}}{A_w} \tag{5}$$

Solving for the area product $(A_c . W_a)$ we have,

$$A_c . W_a = A_{p,1ph} = \frac{V_{rms} I_{rms}}{K_f K_w B_{peak} J_{rms} f_s} \tag{6}$$

Where J_{rms} is the RMS current density of the conductors which is limited by thermal losses in the windings. For three phase inductor, the area product is different from the one indicated in Eq. 6. Since the window utilization is half in the 3-phase core for each coil, therefore, the area product changes to,

$$A_{p,3ph} = 3A_c . \left(\frac{W_a}{2}\right) = 1.5 A_{p,1ph} \tag{7}$$

From Eq. 6, it can be seen that factors, such as peak flux density, RMS current density and fill factor have a strong influence on the area product. The right-hand side shows the electrical parameters whereas left-hand side of Eq. 6 indicates the physical core dimensions. The iron core area relates the flux permeance capabilities whereas the window defines the current conduction capabilities of an inductor which is limited by the conductor's thermal characteristics [4-6, 21].

It is important to note that the area product does not depend on the fundamental supply frequency. However, the core losses are proportional to the frequency squared. Therefore, while sizing an inductor for high frequency $(kHz\ to\ MHz)$ applications, it is required to consider the core flux density lower compared to that of the low frequency $(Hz\ to\ kHz)$ applications [21-22].

IV. 45KW AEROPSACE STARTER-GENERATOR

The radial cross-section and required torque-speed characteristics of the starter-generator are depicted in Fig. 4 and Fig. 5 respectively. Its parameter details are shown in Table I.

The machine works as a motor during engine start and is needed to produce a maximum constant torque from standstill to an engine firing speed of 8000 RPM. Between the speeds of 8000 RPM (ω_{start}) to 20,000 RPM (ω_{min}), the machine supplies the constant power to accelerate the engine. Once the engine reaches its steady state region, the machine acts as a generator between the speeds of 20,000 $RPM(\omega_{min})$ and 32,000 $RPM(\omega_{max})$. In generating mode, the machine generates a maximum power of 45kW up to a maximum speed of 32000 RPM (ω_{max}).

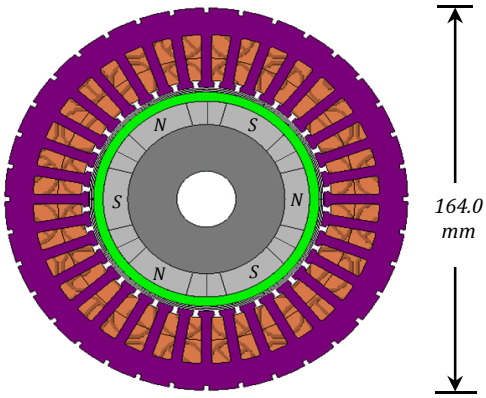

Fig. 4. Radial Corss-section of the Starter-Generator

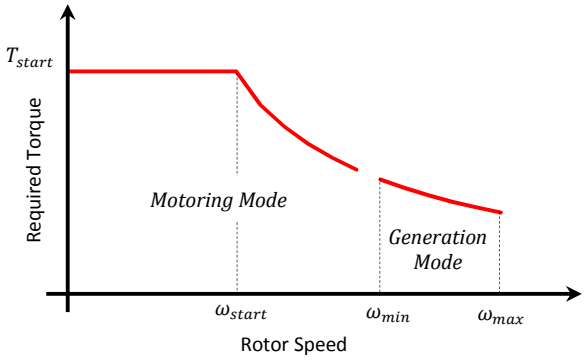

Fig. 5. Torque-speed Characteristics of the Starter-Generator

Since the phase inductance of the starter-generator is low (99 µH), an additional inductance is required to increase the motor side inductance by twice. This increase in inductance will reduce the magnitude of the inverter generated switching ripple by half. Moreover, doubling the motor inductance will also ease the control system design of the starter-generator.

TABLE I. DESIGN DETAILS OF THE STARTER-GENERATOR

PARAMETERS	VALUE	UNIT
Stator Core Material	JFE 10JNEX900	-
Stator Slots and Poles	36/6	-
Cooling System	Liquid	-
Base Speed / Rated Speed	8000	*RPM*
Maximum Speed	32,000	*RPM*
RMS Current at 8000 *RPM*	236.9	A
RMS Current at 20,000 *RPM*	154.4	A
RMS Current at 32,000 *RPM*	188.2	A
RMS Current Density	18	A/mm^2
Active Stack Length	80.2	mm
Inner and Outer Diameter	96/164	mm
Shaft Diameter	4	mm
Phase Resistance @ 30 ^{0}C	13.2	mΩ
Phase Inductance	99	µH

V. INDUCTOR SIZING

Six slot integrated rotor-less inductor with double layer concentrated winding ($DL\ CNW$) is chosen to be designed at RMS current density of 18 A/mm^2 (which is same as the current density of the starter-generator) whereas, the EE core inductor is designed for natural convection cooling system. The core reason of choosing $DL\ CNW$ is to limit the overall volume of the end-windings which was the strict guideline from the starter-generator's point of view.

To size the EE core and the integrated inductor, the area product approach is used. Both inductors are sized by specifying the required synchronous inductance, peak magnetic flux density in the core, fill factor, RMS current density of the conductor and the type of magnetic core material, the details of which are shown in Table II and Table III respectively. However, the RMS current density through the inductor is different for both inductors.

While sizing the inductor, the following design ratios were considered for both integrated and EE core inductors.

- Window to Core Area Ratio, W_a/A_c = 0.7
- Window Length to Height Ratio, G/F = 3
- Stack to Limb Length Ratio, L_{stack}/L_{limb} = 0.77

The author of [6] has suggested to set a low window-to-core area ratio in order to keep the fringing effect at a minimum level. Also, the window length-to-height ratio is selected based on the information provided by the manufacturer in [6]. However, the stack-to-limb ratio is chosen based on the outer diameter limitation of the starter-generator for the integrated one and the same ratio was maintained for EE core inductor.

A. EE Core Inductor

Once the area product is estimated using Eq. 7, the core length ratio (L_{stack}/L_{limb}) and window aspect ratio (G/F) are then chosen to set the stack and limb dimensions and the window dimensions of the core respectively. The number of turns per phase is calculated based on the specified voltage across the inductor. The airgap is fixed to get a required synchronous inductance. So, the number of turns and the airgap length can be determined using,

$$N_{ph} = \frac{V_{rms}}{K_f A_c B_{peak} f_s} \tag{8}$$

$$L_g = \frac{(4\pi \times 10^{-7}) N_{ph}^2 A_c}{L_{synch}} \tag{9}$$

TABLE II. SPECIFICATIONS OF EE CORE INDUCTOR

SPECIFICATIONS	VALUES	UNIT
Core Material	Hiperco 50A 0.014	-
Required Inductance	99	µH
RMS Operating Current	236.9	A
Peak Flux Density	2.3	T
Slot Fill Factor	0.5	-
RMS Current Density	4.8	A/mm^2
Waveform Factor (K_w)	4.44	-

TABLE III. SPECIFICATIONS OF INTEGRATED INDUCTOR

SPECIFICATIONS	VALUES	UNIT
Core Material	Hiperco 50A 0.014	-
Required Inductance	99	µH
RMS Operating Current	236.9	A
Peak Flux Density	2.3	T
Slot Fill Factor	0.5	-
RMS Current Density	18	A/mm2
Waveform Factor (K_w)	4.44	-
Hole for the motor shaft	> 4	mm
Outer Diameter	164	mm

B. Integrated Rotor-less Inductor

The area product of the integrated rotor-less inductor (Fig. 6) is estimated based on the RMS current density as illustrated in Table III. At first, the windows area is fixed to that of EE core inductor along with the identical number of turns. The tooth width is then selected as the limb length (L_{limb})of EE core inductor. This is correct for 6 slots inductor however, for higher number of slots, the tooth width needs to be adjusted in proportion to the total number of slots. The back iron width is adjusted to keep the identical flux density in the core and the slot opening height is increased to keep the uniform flux density throughout the stator slots. Since it is a rotor-less inductor, phase inductance is only controlled by the slot opening unlike integrated rotational inductor in [3, 4]. Fig. 7(a) and Fig. 7(b) shows the cross-section and flux distribution of EE core and integrated rotor-less inductor respectively.

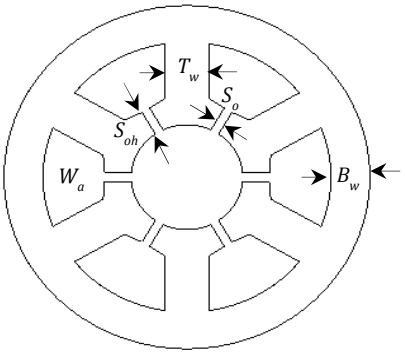

Fig. 6. Physical Layout of Integrated Rotor-less Inductor

VI. COMPARATIVE ANALYSIS

A. Weight and Volume Comparison

Both EE core and integrated inductors are compared in terms of their total weight and volume. The total weight and volume includes: iron core and copper including the end-windings. The end-windings length is calculated using the method described in [4-5]. The comparison of the sizing parameters between the EE core and the integrated inductor is shown in Table IV, whereas its design parameters are illustrated in Table V. Significant reduction in total weight and volume is achieved by sizing the integrated inductor at the same current density of the starter-generator (as expected). As a result, the weight of the integrated inductor is reduced by 55.4%, while its volume is reduced by 52.7% as compared to the traditional EE core inductor.

TABLE IV. SIZING COMPARISON OF EE CORE AND INTEGRATED INDUCTOR

SIZING PARAMETERS	EE CORE INDUCTOR	INTEGRATED INDUCTOR	UNIT
Iron Weight	6.84	2.44	Kg
Copper Weight (With End Windings)	3.10	1.99	Kg
Total Weight (Iron + Copper)	9.94	4.43	Kg
Total Volume (Iron + Copper)	2078	981.8	cm^3

TABLE V. DESIGN PARAMETERS OF EE CORE AND INTEGRATED INDUCTOR

DESIGN PARAMETERS	EE CORE INDUCTOR	INTEGRATED INDUCTOR	UNIT
Area Product	181.6	45.7	cm^4
Synchronous Inductance	90	90	µH
Peak Flux Density	2.2	2.2	T
Phase Resistance @ 30 ^{0}C	1.0	8.2	mΩ
Turns per Phase	10	36	-
Slot Area	1840	925	mm^2
Conductor Diameter	8.0	4.0	mm
Active Stack Length	32	20	mm
Active Stack Length for 99µH	36	22.5	mm
Total Stack Length (With End Windings)	66.8	46.5	mm

The phase resistance of the EE core inductor is 8.2 times lower than that of the integrated inductor due to lower current density. The associated thermal losses are managed by the existing cooling system of the starter-generator which is forced oil cooling (engine oil). The inductance values are validated using the *FE* simulations. The synchronous inductance of 90µH is obtained through *FEA* for both *EE* core and the integrated inductor. The required inductance of 99µH is achieved by adjusting their stack length of the iron core as indicated in Table V.

B. Total Loss, Volume and Weight Comparison

In this section, the total losses, volume and weight of the filter inductor is combined with that of the starter-generator for comparing traditional and integrated systems. The core and copper loss of the EE core inductor, integrated inductor and the starter-generator has been investigated and compared using *FE* models at 8000 *RPM*. This is due to the fact that the copper losses are maximum at this speed which is also a dominant loss component compared to the iron loss.

From Table VI, it can be seen that both volume and weight of the combined system are significantly reduced. The combined volume is reduced by 29.1% while the combined weight is reduced by 25.5% for the integrated inductor as compared to the system with EE core inductor. However, this reduction comes at the expense of extra 0.9 kW loss which is absorbed effectively by the existing cooling system of the starter-generator. The thermal behaviour of the integrated inductor can also be predicted by looking at its losses. Since the integrated inductor is placed axially with the starter-generator, the loss of 1.57KW can easily be handled by the existing cooling system of the starter-generator.

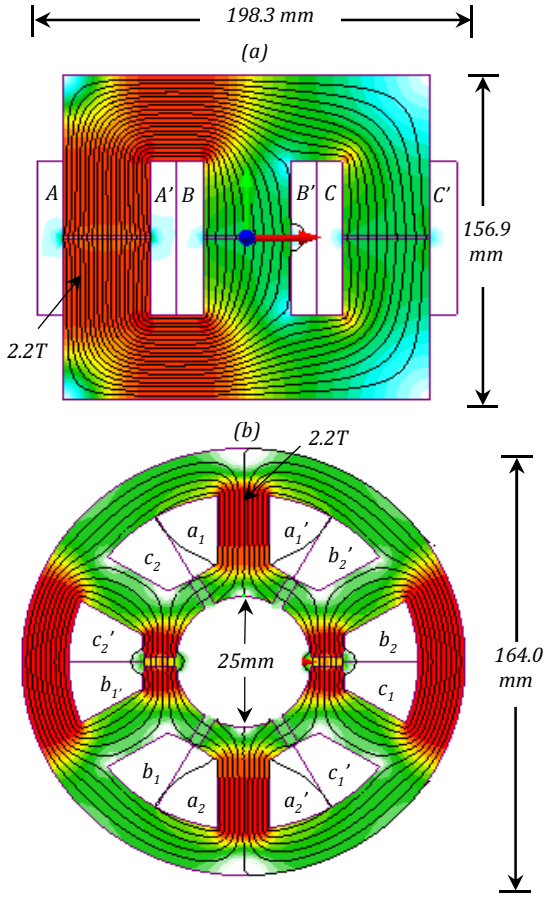

Fig. 7. Radial Cross-section and Flux Distribution (a) EE Core Inductor (b) Integrated Rotor-less Inductor

TABLE VI. CORE AND COPPER LOSS OF INTEGRATED INDUCTOR AND STATER-GENERATOR

PARAMETERS	EE INDUCTOR	INTEGRATED INDUCTOR	STARTER-GENERATOR
Core Loss at 8 kRPM	489.3 W	193 W	86 W
Copper Loss at 8 kRPM	168.5 W	1381W	2223 W
Total Losses	0.658 KW	1.57 KW	2.31 KW
Total Volume	2078 cm^3	981 cm^3	1689 cm^3
Total Weight	9.94 Kg	4.43 Kg	11.7 Kg
Combined Volume (SG + Inductor)	3767 cm^3	2670 cm^3	-
Combined Weight (SG + Inductor)	21.6 Kg	16.1 Kg	-
% Volume Reduction	-	29.1 %	-
% Weight Reduction	-	25.5 %	-

VII. CONCLUSION

An integrated option is adopted to realize a physical integration of passive filter inductor which was required to smooth out the switching ripple component from the current waveforms of the starter-generator. This paper presented a design of an integrated rotor-less inductor for the application of a 45kW aerospace starter-generator. The effect of high current density inductor was investigated and compared with traditional EE core inductor in terms of their total weight and volume. Both the inductors were sized using the area product approach and its design parameters were validated through finite element analysis.

The comparative analysis between the traditional EE core and the integrated inductor has shown a significant reduction in total weight and volume of the system. The total weight of the integrated inductor is reduced by 55.4% whereas the total volume is reduced by 52.7% as compared to a traditional inductor. The total losses, volume and weight were combined with that of the starter-generator for comparing traditional and integrated systems. The combined volume was reduced by 29.1% while the combined weight was reduced by 25.5% when compared to the system with EE core inductor. However, this reduction comes at the expense of an extra 0.9 kW losses which is absorbed by the existing cooling system of the starter-generator.

VIII. FURTHER WORK

The thermal behaviour of the combined integrated inductor and starter-generator system has not been discussed in this paper. A full CFD of the integrated inductor at different operating points would be ideal to predict its thermal behaviour.

ACKNOWLEDGEMENT

This work was supported by the Ningbo Science & Technology Bureau under Grant 2013A31012 and by the Ningbo Science & Technology Bureau under Grant 2014A35007.

IX. REFERENCES

[1] Robert Abebe, Gaurang Vakil, Giovanni Lo Calzo, Thomas Cox, Simon Lambert, Mark Johnson, Chris Gerada, Barrie Mecrow "Integrated motor drives: state of the art and future trends" IET Electric Power Applications, 15 pp, Print ISSN 1751-8660, Online ISSN 1751-8679

[2] M. Raza Khowja, C. Gerada, G. Vakil, P. Wheeler and C. Patel, "Integrated output filter inductor for permanent magnet motor drives," IECON 2016 - 42nd Annual Conference of the IEEE Industrial Electronics Society, Florence, 2016

[3] M. Raza Khowja, C. Gerada, G. Vakil, P. Wheeler and C. Patel, "Novel integrative options for passive filter inductor in high speed AC drives," IECON 2016 - 42nd Annual Conference of the IEEE Industrial Electronics Society, Florence, 2016

[4] M. Raza Khowja, C. Gerada, G. Vakil, C. Patel and P. Wheeler, "Design optimization of integrated rotational inductors for high-speed AC drive applications," 2017 IEEE International Electrical Machine & Drives Conference (IEMDC), Miami FL, USA, 2017

[5] M. Raza Khowja, C. Gerada, G. Vakil, C. Patel and P. Wheeler, "Design optimization of integrated rotor-less inductors for high-speed AC drive applications," 2017 IEEE Workshop on Electrical Machines Design, Control and Diagnosis (WEMDCD), Nottingham, United Kingdom, 2017

[6] Colonel Wm. T. Mclyman "Transformer and Inductor Design Handbook", Fourth Edition

[7] Naayagi R.T, Forsyth A.J. "Design of high frequency air-core inductor for DAB converter" Power Electronics, Drives and Energy Systems (PEDES), 2012 IEEE International Conference. Publication Year: 2012 , Page(s): 1 – 4

[8] Meere R, Ningning Wang, O'Donnell T, Kulkarni S, Roy S, O'Mathuna, S.C. "Magnetic-Core and Air-Core Inductors on Silicon: A PerformanceComparison up to 100 MHz" Magnetics, IEEE Transactions. Publication Year: 2011 , Page(s): 4429 – 4432

[9] Nee B.M, Chapman P.L. "Integrated Filter Element in Electric Drives" Vehicle Power and Propulsion Conference, 2007. VPPC 2007. IEEE. Publication Year: 2007 , Page(s): 148 - 153

[10] Garvey S.D. Norris, W.T, Wright M.T. "The role of integrated components in protecting motor windings". Electric Power Applications, IEEE Proceedings - Volume: 147 , Issue: 5 Publication Year: 2000, Page(s): 367 - 370

[11] Nakajima, Yuki Imazu, Tomoya Mizukoshi, Yukio Sato, Sho Zushi, Yusuke "Integrated Capacitor Type Stator", Patent No. 8049383

[12] Chen R, van Wyk J.D, Wang S, Odendaal W.G. "Planar electromagnetic integration technologies for integrated EMI filters". Industry Applications Conference, 2003. 38th IAS Annual Meeting. Conference Record of the Volume: 3. Publication Year: 2003, Page(s): 1582 - 1588 vol.3

[13] Fang Luo, Robutel R, Shuo Wang, Wang F, Boroyevich D. "Integrated Input EMI Filter for a 2 kW DC-fed 3-phase Motor Drive". Applied Power Electronics Conference and Exposition, 2009. APEC 2009. Twenty-Fourth Annual IEEE. Publication Year: 2009, Page(s): 325 – 329

[14] Chen R, Shuo Wang, van Wyk J.D, Odendaal W.G. "Integration of EMI filter for distributed power system (DPS) front-end converter" Power Electronics Specialist Conference, 2003. PESC '03. 2003 IEEE 34th Annual Volume: 1 Publication Year: 2003 , Page(s): 296 - 300 vol.1

[15] Zhao L, Strydom J.T, van Wyk J.D. "Wide band modelling of integrated passive structure: the series resonator". Power Electronics Specialists Conference, 2002. pesc 02. 2002 IEEE 33rd Annual Volume:3. Publication Year: 2002 , Page(s): 1283 - 1288 vol.3

[16] Lingyin Zhao Strydom J.T, van Wyk J.D. "An alternative planar multi-cell structure integrated reactive module" Industry Applications Conference, 2001. Thirty-Sixth IAS Annual Meeting. Conference Record of the 2001 IEEE Volume: 4 Publication Year: 2001 , Page(s): 2217 - 2223 vol.4

[17] Chen R, Strydom J.T, van Wyk J.D. "Design of planar integrated passive module for zero-voltage switched asymmetrical half bridge PWM converter" Industry Applications, IEEE Transactions on Volume: 39, Publication Year: 2003 , Page(s): 1648 - 1655

[18] Strydom J.T, van Wyk J.D, Ferreira J.A. "Some limits of integrated LCT modules for resonant converters at 1 MHz" Industry Applications Conference, 1999. Thirty-Fourth IAS Annual Meeting. Conference Record of the 1999 IEEE. Publication Year: 1999 , Page(s): 1411 - 1417

[19] Popovic-Gerber Jelena, Gerber M, Ferreira Braham "Integrated filter in electrolytic capacitor technology for implementation in high power density idustrial drives" Power Electronics Specialists Conference, 2008. PESC 2008. IEEE. Publication Year: 2008 , Page(s): 2968 - 2974

[20] Popovic J, Ferreira J.A, Gerber M.B, Konig A, de Doncker, R. "Integration technologies for high power density power electronic converters for AC drives". Power Electronics, Electrical Drives, Automation and Motion, 2006. SPEEDAM 2006. Publication Year: 2006 , Page(s): 634 - 639

[21] Kazimierczuk M.K, Sekiya H. "Design of AC resonant inductors using area product method" Energy Conversion Congress and Exposition, 2009. ECCE 2009. IEEE Publication Year: 2009

[22] H. Nijende, N. Frohleke and J. Bocker, "Optimized size design of integrated magnetic components using area product approach," 2005 European Conference on Power Electronics and Applications, Dresden, 2005, pp. 10 pp.-P.10.